Electrochemical and IR/UV−Vis Spectroelectrochemical Studies of *fac*-[Mn(X)(CO)$_3$(iPr-DAB)]^n (n = 0, X = Br, Me, Bz; n = +1, X = THF, MeCN, nPrCN, P(OMe)$_3$; iPr-DAB = 1,4-Diisopropyl-1,4-diaza-1,3-butadiene) at Variable Temperatures: Relation between Electrochemical and Photochemical Generation of [Mn(CO)$_3$(α-diimine)]$^-$

Brenda D. Rossenaar,[†] František Hartl,*[,†] Derk J. Stufkens,[†] Christian Amatore,[‡] Emmanuel Maisonhaute,[‡] and Jean-Noël Verpeaux[‡]

Anorganisch Chemisch Laboratorium, J. H. van't Hoff Research Instituut, Universiteit van Amsterdam, Nieuwe Achtergracht 166, 1018 WV Amsterdam, The Netherlands, and Ecole Normale Supérieure, Département de Chimie, URA CNRS 1679, 24 rue Lhomond, 75231 Paris Cedex 05, France

Received April 2, 1997[⊗]

The title complexes [Mn(X)(CO)$_3$(iPr-DAB)]^n (n = 0, X = Br; n = +1, X = donor solvent) undergo a two-electron reduction according to an ECE sequence. The chemical step (C) involves prompt dissociation of the X ligand from the primary one-electron reduction product, followed by instantaneous one-electron reduction of the five-coordinate transient [Mn(CO)$_3$(iPr-DAB)]$^\bullet$ producing the anion [Mn(CO)$_3$(iPr-DAB)]$^-$. The latter complex remains rather stable at T < 190 K, whereas at higher temperatures it undergoes an electron-transfer reaction with the parent complexes producing the dimer [Mn(CO)$_3$(iPr-DAB)]$_2$ (the second C step in the overall ECEC sequence). The rate of this reaction decreases in the order THF > MeCN > Br. The driving force for this behavior is the more positive $E_{1/2}$ value of the redox couple [Mn(CO)$_3$(iPr-DAB)]$^{\bullet/-}$ relative to those of [Mn(Br)(CO)$_3$(iPr-DAB)]$^{0/\bullet-}$ and [Mn(X)(CO)$_3$(iPr-DAB)]$^{+/\bullet}$ (X = donor solvent) and a very short lifetime of the primary reduction products. In contrast, the ligand P(OMe)$_3$ in [Mn{P(OMe)$_3$}(CO)$_3$(iPr-DAB)]$^\bullet$ is bound rather firmly at low temperatures, where the ECE sequence to [Mn(CO)$_3$(iPr-DAB)]$^-$ *via* [Mn(CO)$_3$(iPr-DAB)]$^\bullet$ is only a minor route. The reduction of [Mn(X)(CO)$_3$(iPr-DAB)] (X = Me, Bz) at room temperature affords the five-coordinate anion [Mn(CO)$_3$(iPr-DAB)]$^-$ *via* dissociation of X$^\bullet$ from the one-electron-reduced intermediate [Mn(X)(CO)$_3$(iPr-DAB)]$^{\bullet-}$ detectable by cyclic voltammetry for X = Me. Oxidation of the five-coordinate anion [Mn(CO)$_3$(iPr-DAB)]$^-$ produces the dimer [Mn(CO)$_3$(iPr-DAB)]$_2$, following the *reverse* ECE(C) sequence involved in the reduction path. The direct dimerization of the radicals primarily formed, [Mn(CO)$_3$(iPr-DAB)]$^\bullet$, is probably only a minor alternative route. In the presence of excess P(OMe)$_3$, the principal oxidation product is the cation [Mn{P(OMe)$_3$}(CO)$_3$(iPr-DAB)]$^+$. The five-coordinate anions [Mn(CO)$_3$(α-diimine)]$^-$ can be regarded as strongly π-delocalized complexes with the negative charge equally distributed over the α-diimine and CO ligands. The intriguing mechanism of their *photochemical* formation from *fac*-[Mn(Br)(CO)$_3$(α-diimine)] at low temperatures has been rectified on the basis of this (spectro)electrochemical study.

Introduction

Carbonyl complexes of the type [Re(X)(CO)$_3$(α-diimine)]$^{0/+}$ (X = CO, halide, alkyl, organic donor) have been the subject of many photochemical,[1] photophysical,[2] and electrochemical[3] studies, mainly due to their capability of mediating inter- and intramolecular electron-transfer reactions. Even though there are quite a few reports on the photochemistry of the Mn derivatives [Mn(X)(CO)$_3$(α-diimine)] (X = halide,[4−6] alkyl,[7] metal fragment[8−11]), electrochemical studies of these com-

[†] Universiteit van Amsterdam.
[‡] Ecole Normale Supérieure.
[⊗] Abstract published in *Advance ACS Abstracts,* September 15, 1997.

(1) For example, see: (a) Lucia, L. A.; Burton, R. D.; Schanze, K. S. *Inorg. Chim. Acta* **1993**, *208*, 103. (b) Rossenaar, B. D.; Kleverlaan, C. J.; van de Ven, M. C. E.; Stufkens, D. J.; Vlček, A., Jr. *Chem. Eur. J.* **1996**, *2*, 228. (c) Hori, H.; Johnson, F. P. A.; Koike, K.; Ibusuki, T.; Ishitani, O. *J. Chem. Soc., Dalton Trans.* **1997**, 1019 and references therein.

(2) For example, see: (a) Kalyanasundaram, K. *Photochemistry of Polypyridine and Porphyrin Complexes*; Academic Press, New York, 1992. (b) Schanze, K. S.; MacQueen, D. B.; Perkins, T. A.; Cabana, L. A. *Coord. Chem. Rev.* **1993**, *122*, 63. (c) Shaver, R. J.; Perkovic, M. W.; Rillema, D. P.; Woods, C. *Inorg. Chem.* **1995**, *34*, 5446 and references therein. (d) Baiano, J. A.; Murphy, W. R., Jr. *Inorg. Chem.* **1991**, *30*, 4594 and references therein. (e) Kleverlaan, C. J.; Martino, D. M.; van Willigen, H.; Stufkens, D. J.; Oskam, A. *J. Phys. Chem.* **1996**, *100*, 18607.

(3) For example, see: (a) Stor, G. J.; Hartl, F.; van Outersterp, J. W. M.; Stufkens, D. J. *Organometallics* **1995**, *14*, 1115. (b) Johnson, F. P. A.; George, M. W.; Hartl, F.; Turner, J. J. *Organometallics* **1996**, *15*, 3374 and references therein. (c) Shaver, R. J.; Rillema, D. P. *Inorg. Chem.* **1992**, *31*, 4101. (d) Lee, Y. F.; Kirchhoff, J. R.; Berger, R. M.; Gosztola, D. *J. Chem. Soc., Dalton Trans.* **1995**, 3677. (e) Klein, A.; Vogler, C.; Kaim, W. *Organometallics* **1996**, *15*, 236.

(4) Stor, G. J.; Morrison, S. L.; Stufkens, D. J.; Oskam, A. *Organometallics* **1994**, *13*, 2641.

S0276-7333(97)00279-3 CCC: $14.00

plexes are scarce.[12−14] Recently, we presented a spectroelectrochemical study[13] of $[Mn(Cl)(CO)_3(bpy)]$[15] with the major goal of explaining the mechanism of the formation of the five-coordinate anion $[Mn(CO)_3(bpy)]^-$ on irradiation of *fac*-$[Mn(Br)(CO)_3(\alpha\text{-diimine})]$ in 2-MeTHF at 153 K.[4] In situ IR/UV−vis spectroelectrochemical experiments at room temperature revealed that the reduction of $[Mn(Cl)(CO)_3(bpy)]$ produced, exclusively, the dimer $[Mn(CO)_3(bpy)]_2$, which converted in the subsequent cathodic step to the stable anion $[Mn(CO)_3(bpy)]^-$. At 223 K, however, $[Mn(CO)_3(bpy)]^-$ was produced simultaneously with $[Mn(CO)_3(bpy)]_2$. This observation was tentatively attributed to inhibited dimerization of the five-coordinate radicals $[Mn(CO)_3(bpy)]^\bullet$ at temperatures below 220 K,[11c] which allowed their direct reduction to $[Mn(CO)_3(bpy)]^-$. We have recently found, however, that the dimer $[Mn(CO)_3(bpy)]_2$ may also result from a coupling reaction between equivalent amounts of $[Mn(CO)_3(bpy)]^-$ and parent $[Mn(Cl)(CO)_3(bpy)]$. This result points to an alternative route to $[Mn(CO)_3(bpy)]_2$ *via* an ECEC sequence described by eqs 1−4. In this sequence, the dimerization of reducible

$$[Mn(Cl)(CO)_3(bpy)] + e^- \leftrightarrows [Mn(Cl)(CO)_3(bpy)]^{\bullet -} \quad (1)$$

$$[Mn(Cl)(CO)_3(bpy)]^{\bullet -} \rightarrow [Mn(CO)_3(bpy)]^\bullet + Cl^- \quad (2)$$

$$[Mn(CO)_3(bpy)]^\bullet + e^- \leftrightarrows [Mn(CO)_3(bpy)]^- \quad (3)$$

$$[Mn(Cl)(CO)_3(bpy)] + [Mn(CO)_3(bpy)]^- \rightarrow [Mn(CO)_3(bpy)]_2 + Cl^- \quad (4)$$

$[Mn(CO)_3(bpy)]^\bullet$ cannot compete[16] with the electrochemical reduction described by eq 3, as erroneously anticipated.[13]

In this work, we describe the electrochemical reduction of the corresponding complexes *fac*-$[Mn(X)(CO)_3(iPr\text{-}DAB)]^n$ ($n = 0$, X = Otf, Br, Me, Bz; $n = +1$, THF, MeCN, nPrCN). Perusal of these results allows us to rectify the inaccurate[13] mechanisms of the electrochemical and photochemical formation of the five-coordinate anions $[Mn(CO)_3(\alpha\text{-diimine})]^-$. Our interest in the electrochemical reduction of the complexes $[Mn(X)(CO)_3(iPr\text{-}DAB)]$ (X = Me, Bz) relates to the one-electron reduction of the Re derivatives, which produces remarkably stable radical anions $\{[Re(CO)_3(iPr\text{-}DAB)]^-\cdots X^\bullet\}$ (X = Me, Et, Bz).[17]

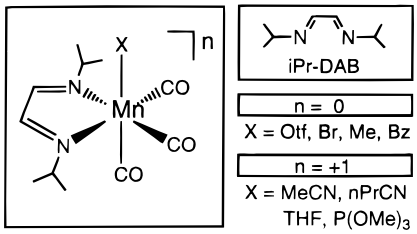

Figure 1. General molecular structure of the complexes studied.

The structure of the title complexes *fac*-$[Mn(X)(CO)_3(iPr\text{-}DAB)^n$ is schematically depicted in Figure 1.

Experimental Section

Chemicals. The solvents nPrCN (Fluka), MeCN (Acros Chimica), and THF (Acros Chimica)[15] were dried on CaH_2 (nPrCN and MeCN) or Na wire (THF) and distilled under nitrogen prior to use. The supporting electrolytes Bu_4NPF_6 (Fluka) and Bu_4NBF_4 (prepared from Bu_4NHSO_4 and $NaBF_4$) were dried overnight under vacuum at 353 K and stored under argon before use. PPh_3 (Aldrich) was recrystallized from a diethylether solution at 223 K. $P(OMe)_3$ (Aldrich) was distilled from CaH_2 under nitrogen before use. Ferrocene (BDH) and Ag^+Otf^- (Aldrich)[15] were used as received.

The complexes $[Mn(X)(CO)_3(iPr\text{-}DAB)]$ (X = Br,[18] Otf,[11a] Me,[7] Bz[7]) were synthesized according to literature procedures and purified by column chromatography over Silica 60 (Merck), activated by heating overnight under vacuum at 433 K, with a gradient elution of *n*-hexane/THF. The purity of the complexes was checked by mass, UV−vis, IR, and ^1H NMR spectroscopies.

The spectroelectrochemical samples were carefully prepared under an atmosphere of high-purity nitrogen or argon, using Schlenk techniques. The solutions of the light-sensitive complexes $[Mn(X)(CO)_3(iPr\text{-}DAB)]$ (X = Me, Bz) were handled in the dark. The complexes $[Mn(X)(CO)_3(iPr\text{-}DAB)]$ (X = Otf, Br) are less photoreactive than the alkyl complexes, but still demanding the use of light-protected cells.

Spectroelectrochemical Measurements and Instrumentation. IR spectra were recorded on a Bio-Rad FTS-7 FTIR spectrometer (16 scans, resolution of 2 cm^{-1}). Electronic absorption spectra were measured on a Perkin-Elmer Lambda 5 UV−vis spectrophotometer, attached to a 3600 data station. IR and UV−vis spectroelectrochemical measurements at room temperature were performed in an OTTLE cell,[19] equipped with a Pt minigrid working electrode (32 wires/cm) and CaF_2 optical windows. For IR and UV−vis spectroelectrochemistry at low temperatures, we employed a purpose-made OTTLE cell[20] which fitted into a liquid-nitrogen cryostat.[21] A PA4 potentiostat (EKOM, Czech Republic) was used to carry out the controlled-potential electrolyses. The solutions were typi-

(5) Rosa, A.; Ricciardi, G.; Baerends, E. J.; Stufkens, D. J. *J. Phys. Chem.* **1996**, *100*, 15346.
(6) Kleverlaan, C. J.; Hartl, F.; Stufkens, D. J. *J. Photochem. Photobiol., A* **1997**, *103*, 231.
(7) Rossenaar, B. D.; Stufkens, D. J.; Oskam, A.; Fraanje, J.; Goubitz, K. *Inorg. Chim. Acta* **1996**, *247*, 215.
(8) Andréa, R. R.; de Lange, W. G. J.; Stufkens, D. J.; Oskam, A. *Inorg. Chem.* **1989**, *28*, 318.
(9) Rossenaar, B. D.; van der Graaf, T.; van Eldik, R.; Langford, C. H.; Stufkens, D. J.; Vlček A., Jr. *Inorg. Chem.* **1994**, *33*, 2865.
(10) van der Graaf, T.; Stufkens, D. J.; Oskam, A.; Goubitz, K. *Inorg. Chem.* **1991**, *30*, 599.
(11) (a) Kokkes, M. W.; de Lange, W. G. J.; Stufkens, D. J.; Oskam, A. *J. Organomet. Chem.* **1985**, *294*, 59. (b) Kokkes, M. W.; Stufkens, D. J.; Oskam, A. *Inorg. Chem.* **1985**, *24*, 4411. (c) Kokkes, M. W.; Stufkens, D. J.; Oskam, A. *Inorg. Chem.* **1985**, *24*, 2934.
(12) van der Graaf, T.; Hofstra, R. M. J.; Schilder, P. G. M.; Rijkhoff, M.; Stufkens, D. J.; van der Linden, J. G. M. *Organometallics* **1991**, *10*, 3668.
(13) Hartl, F.; Rossenaar, B. D.; Stor, G. J.; Stufkens, D. J. *Recl. Chim. Pays-Bas* **1995**, *114*, 565.
(14) Brown, N. C.; Carriedo, G. A.; Connelly, N. G.; Garcia Alonso, F. J.; Quarmby, I. C.; Rieger, A. L.; Rieger, P. H.; Riera, V.; Vivanco, M. *J. Chem. Soc., Dalton Trans.* **1994**, 3745.
(15) The abbreviations used stand for bpy = 2,2′-bipyridine, iPr-DAB = 1,4-diisopropyl-1,4-diaza-1,3-butadiene, iPr-PyCa = pyridine-2-carbaldehyde 1-isopropylimine, DBCat = 3,5-di-*tert*-butyl-1,2-benzocatecholate; Me = methyl, Bz = benzyl; nPrCN = butyronitrile, MeCN = acetonitrile, THF = tetrahydrofuran; Fc/Fc^+ = ferrocene/ferrocenium; Otf = $CF_3SO_3^-$; OTTLE = optically transparent thin-layer electrochemical; SCE = saturated calomel electrode.
(16) Amatore, C.; Savéant, J. M. *J. Electroanal. Chem., Interfacial Electrochem.* **1981**, *125*, 1.
(17) Rossenaar, B. D.; Hartl, F.; Stufkens, D. J. *Inorg. Chem.* **1996**, *35*, 6194.
(18) Staal, L. H.; Oskam, A.; Vrieze, K. *J. Organomet. Chem.* **1979**, *170*, 235.
(19) Krejčík, M.; Daněk, M.; Hartl, F. *J. Electroanal. Chem., Interfacial Electrochem.* **1991**, *317*, 179.
(20) Hartl, F.; Luyten, H.; Nieuwenhuis, H. A.; Schoemaker, G. *Appl. Spectrosc.* **1994**, *48*, 1522.
(21) Andréa, R. R.; Luyten, H.; Vuurman, M. A.; Stufkens, D. J.; Oskam, A. *Appl. Spectrosc.* **1986**, *40*, 1184.

Table 1. IR ν(CO) and UV−Vis Data for *fac*-[Mn(X)(CO)$_3$(iPr-DAB)]^n (n = 0, X = Br, Otf, Me, Bz; n = +1, X = nPrCN, P(OMe)$_3$) and Their Reduction Products (in nPrCN, unless Stated Otherwise)

complex	T [K]	ν(CO) [cm^{-1}]	k_{av} [Nm^{-1}]	λ_{max} (ϵ_{max}) [nm] ([cm^{-1} M^{-1}])
[Mn(Otf)(CO)$_3$(iPr-DAB)]	293	2041 (s), 1939 (s,br)[a,b]	1573	
	293	2040 (s), 1954 (s), 1934 (s)[a]	1578	
[Mn(Br)(CO)$_3$(iPr-DAB)]	293	2024 (s), 1934 (m), 1924 (m)	1553	477 (2650)
[Mn(Me)(CO)$_3$(iPr-DAB)]	293	1989 (s), 1897 (s,br)	1501	495 (4600), 343
[Mn(Bz)(CO)$_3$(iPr-DAB)]	293	1990 (s), 1900 (s,br)	1505	502 (5100)
[Mn(nPrCN)(CO)$_3$(iPr-DAB)]$^+$	293	2046 (s), 1955 (s,br)	1593	405 (3000)
	198	2046 (s), 1961 (m), 1946 (m)	1591	401, 355 (sh)
[Mn{P(OMe)$_3$}(CO)$_3$(iPr-DAB)]$^+$	293	2047 (s), 1977 (m), 1943 (m)	1598	
	198	2047 (s), 1976 (m), 1941 (s)	1597	396 (3600), 342 (sh)
[Mn{P(OMe)$_3$}$_2$(CO)$_2$(iPrDAB)]$^+$	293	1969 (s), 1899 (s)	1511	
P$_1$[c]	293	2023 (s), ∼1925 (br)	1554	
[Mn{P(OMe)$_3$}(CO)$_3$(iPr-DAB)]$^\bullet$	198	2017 (s), 1932 (s), 1894 (s)[d]	1533	460 (2000), 380,360,300
[Mn(THF)(CO)$_3$(iPr-DAB)]$^\bullet$ [e]	293	2004 (s), 1914 (vs), 1894 (vs)[a]	1517	
[Mn(CO)$_3$(iPr-DAB)]$_2$	293	1975 (w), 1945 (s), 1886 (m,br)		744 (9650), 550, 480, 370
	293	1977 (w), 1959 (sh,vw), 1948(s) 1896 (sh,w), 1887 (m)[a]		
[Mn(CO)$_3$(iPr-DAB)]$^-$	293	1919 (s), 1811 (s,br)	1379	490 (9300), 392 (6550)
	293	1919 (s), 1822 (s), 1778 (s)[a,f]	1368	485, 386
	198	1923 (s), 1815 (s,br)	1385	483, 386

[a] In THF. [b] In the presence of Bu_4NPF_6. [c] An unidentified side product. [d] ν(CO) bands of the corresponding radical [Mn{P(OMe)$_3$}(CO)$_3$(iPr-PyCa)]$^\bullet$ (iPr-PyCa is defined in see ref 15) found at 2024 (s), 1942 (s) and 1909 (s) cm^{-1} (135 K, 2-MeTHF).[4] [e] Reference 7. [f] As the Na$^+$ salt.

cally 3 × 10^{-1} M in supporting electrolyte and 5 × 10^{-3}−10^{-2} M in the Mn complexes.

Cyclic Voltammetry and Chronoamperometry. Conventional cyclic voltammograms were recorded at 293 and 223 K in a light-protected CV cell equipped with a Pt disk working electrode of 500 μm diameter (polished carefully with a 0.25 μm diamond paste between scans), Pt gauze or coiled Pt wire auxiliary electrodes, and SCE (Tacussel) or a coiled Ag wire normal reference and pseudoreference electrodes, respectively. (Notably, all of the Mn complexes under study strongly adsorb at Au disk electrodes.) The redox potentials are reported against the standard[22] Fc/Fc$^+$ redox couple used as an internal reference. $E_{1/2}$ (Fc/Fc$^+$) was found at +0.425 and +0.575 V *vs* SCE in MeCN and THF, respectively. The solutions for cyclic voltammetric and chronoamperometric experiments were typically 2 × 10^{-3} M in the Mn complexes and 3 × 10^{-1} M in the supporting electrolyte. A homemade potentiostat equipped with positive feedback for ohmic-drop compensation was used.[23] The potential wave forms were provided by an EG & G PAR model 175 signal generator. A Nicolet 3091 digital oscilloscope was used to digitally store the voltammograms or chronoamperograms and to measure their current and potential characteristics. The scan rate v varied between 0.05 and 500 V/s. Steady-state voltammograms were recorded with a homemade 20 μm diameter Pt disk ultramicroelectrode at v = 0.02 V/s.

Ultrafast cyclic voltammetric experiments (for v ranging between 5 × 10^3 and 4 × 10^5 V/s) were performed with a homemade 10 μm diameter Pt disk ultramicroelectrode which was initially polished with carborundum (PRESI P1200) and finally with 0.3 μm alumina (water suspension, PRESI). The reference electrode was a Pt wire. At the end of the experiment, ferrocene was added to the solution for calibration. The auxiliary electrode was a Pt spiral of *ca.* 1 cm^2 surface area. It was placed within a 1 cm distance from the working electrode, facing it. The same potentiostat[23] was used. The signal generator and digital oscilloscope were, in this case, a HP-3314A and a two-channel HP-54510A (8 bits; 1 ns dwell time; 250 MHz), respectively.

Determination of the Apparent Number of Electrons (n_{app}) Consumed during the Reduction of [Mn(X)(CO)$_3$(iPr-DAB)]$^+$ (X = THF, MeCN) and [Mn(Br)(CO)$_3$(iPr-DAB)] (in THF and MeCN). Electron consumption in the transient electrochemistry was determined employing a previously described combination of chronoamperometry and steady-state voltammetry at ultramicroelectrodes.[24] The following solutions (S) were investigated, using ferrocene as the reference compound: S$_a$ (2.00 × 10^{-3} M [Mn(Br)(CO)$_3$(iPr-DAB)] and 1.21 × 10^{-3} M Fc in THF); S$_b$ (1.97 × 10^{-3} M [Mn(Br)(CO)$_3$(iPr-DAB)] and 0.91 × 10^{-3} M Fc in MeCN); S$_c$ (1.95 × 10^{-3} M [Mn(THF)(CO)$_3$(iPr-DAB)]$^+$ and 1.02 × 10^{-3} M Fc in THF); S$_d$ (2.02 × 10^{-3} M [Mn(MeCN)(CO)$_3$(iPr-DAB)]$^+$ and 1.29 × 10^{-3} M Fc in MeCN). For all of these solutions, the supporting electrolyte was 3 × 10^{-1} M Bu_4NBF_4.

(a) Chronoamperometry at a Pt Disk Electrode (d = 500 μm). At zero time, the electrode potential was stepped 200, 250, and 300 mV negatively behind the $E_{p,c}$ value of the parent Mn complexes (see Table 2) or positively behind the $E_{p,a}$ value of Fc (*i.e.*, on the diffusion plateau of the corresponding waves). The pulse duration θ (the characteristic time T_c) was varied between 50 and 300 ms. After $T_c = \theta$ had elapsed, the potential was stepped back to the rest value and the solution was stirred. For each potential step and pulse duration θ, the experiment was repeated independently three times in the sequence Fc(ox)−Mn(red)−Fc(ox). The sets of currents I_{Mn} and I_{Fc} read at T_c were compared to ensure that no fouling of the Pt disk electrode occurred. The Pt disk was carefully repolished before each θ variation.

The following averaged values of R_{chrono} ($=(I_{Mn}/I_{Fc})(c_{Fc}/c_{Mn}) = n_{app}(D_{Mn}/D_{Fc})^{1/2}$)[24] were obtained for the four solutions under study: $R_{chrono}(S_a) = 1.42 \pm 0.03$; $R_{chrono}(S_b) = 1.44 \pm 0.03$; $R_{chrono}(S_c) = 0.59 \pm 0.05$; $R_{chrono}(S_d) = 1.35 \pm 0.05$.

(b) Steady-State Voltammetry and Chronoamperometry at a Pt Disk Ultramicroelectrode ($d = 2r$ = 20 μm). The chronoamperometric experiments as described above were then performed with the Pt disk ultramicroelectrode. In this case, the potential pulse duration θ reached 1.5 s. With such a value, $\theta >> (r^2/D)$ and the resulting spheric diffusion regime implies that the chronoamperometric currents I_{Mn} and I_{Fc} measured in this case are equal to the limiting currents, $I_{L,Mn}$ and $I_{L,Fc}$, of the corresponding steady-state voltammograms recorded with v = 20 mV/s. This relation was confirmed in the case of the ferrocene oxidation. The substitution of the steady-state voltammetry[24] by chronoamperometry was necessary, owing to strong adsorption of all of the Mn complexes under study at the Pt ultramicroelectrode, which resulted in erroneous voltammetric responses. The value of $I_{L,Fc}$ was, therefore, determined *prior* to and after each negative potential

(22) Gritzner, G.; Kuta, J. *Pure Appl. Chem.* **1984**, *56*, 461.
(23) Amatore, C.; Lefrou, C.; Pflüger, F. *J. Electroanal. Chem., Interfacial Electrochem.* **1989**, *270*, 43.
(24) Amatore, C.; Azzabi, M.; Calas, P.; Jutand, A.; Lefrou, C.; Rollin, Y. *J. Electroanal. Chem., Interfacial Electrochem.* **1990**, *288*, 45.

Table 2. Redox Potentials (V *vs* $E_{1/2}$ (Fc/Fc^+)) of *fac*-[Mn(X)(CO)$_3$(iPr-DAB)]^n (n = 0, X = Br, Me, Bz; n = +1, X = nPrCN, MeCN, THF, P(OMe)$_3$, PPh$_3$) and Their Reduction Products[a]

complex	$E_{p,c}$[d]	$E_{p,a}$[e]
[Mn(Br)(CO)$_3$(iPr-DAB)]	−1.57[a,b,c,f]	+0.72[b,f]
	−1.68[c,g]	
[Mn(Me)(CO)$_3$(iPr-DAB)]	−2.02[c,f]	+0.04[c,f]
[Mn(Bz)(CO)$_3$(iPr-DAB)]	−1.90[c,f]	+0.19[c,f]
[Mn(THF)(CO)$_3$(iPr-DAB)]$^+$ [h]	−1.19[a,f]	
[Mn(MeCN)(CO)$_3$(iPr-DAB)]$^+$ [i]	−1.26[b,f]	
[Mn(nPrCN)(CO)$_3$(iPr-DAB)]$^+$ [j]	−1.29[c,f]	
	−1.38[c,g]	
[Mn(PPh$_3$)(CO)$_3$(iPr-DAB)]$^+$ [k]	−1.28[a,f]	
[Mn{P(OMe)$_3$}(CO)$_3$(iPr-DAB)]$^+$	−1.36[c,f]	
[Mn{P(OMe)$_3$}$_2$(CO)$_2$(iPr-DAB)]$^+$	−1.66[c,f,l]	
[Mn{P(OMe)$_3$}(CO)$_3$(iPr-DAB)]$^\bullet$	−2.38[c,f,l]	
[Mn(CO)$_3$(iPr-DAB)]$_2$	−1.73[a,f]	
	−1.64[b,f]	−0.24[a,b,c,f]
	−1.66[c,f]	
[Mn(CO)$_3$(iPr-DAB)]$^-$		−1.19[a,c,f]
		−1.15[b,f]
		−0.95[c,g]
[Mn(Cl)(CO)$_3$(bpy)][m]	−1.89[a,f]	
[Mn{P(OMe)$_3$}(CO)$_3$(bpy)]$^+$ [n]	−1.78[a,f]	
[Mn(CO)$_3$(bpy)]$_2$[m]	−2.05[a,f]	−0.61[a,f]
[Mn(CO)$_3$(bpy)]$^-$ [m]		−1.53[a,f]

[a] The redox potentials of corresponding bpy-complexes are included for comparison. Conditions and definitions: Cyclic voltammetry; 2×10^{-3} M solutions in THF containing 3×10^{-1} M Bu_4NPF_6; v = 100 mV/s, Pt disk working electrode. $E_{1/2}$ (Fc/Fc^+) = +0.575 V *vs* SCE. [b] Same conditions as *a* except in MeCN. $E_{1/2}$ (Fc/Fc^+) = +0.425 V *vs* SCE. [c] Same conditions as *b* except in nPrCN. [d] Reduction of the complex; $E_{p,c}$ = cathodic peak potential. [e] Irreversible oxidation of the complex; $E_{p,a}$ = anodic peak potential. [f] At 293 K. [g] At 223 K. [h] Solution of [Mn(Otf)(CO)$_3$(iPr-DAB)] in THF. [i] Solution of [Mn(Otf)(CO)$_3$(iPr-DAB)] in MeCN. [j] Solution of [Mn(Otf)(CO)$_3$(iPr-DAB)] in nPrCN. [k] Solution of [Mn(Otf)(CO)$_3$-(iPr-DAB)] in THF/excess PPh$_3$. [l] ΔE_p = 100 mV. [m] From ref 13. [n] From ref 14.

step to reduce the Mn complexes. Reliable $I_{L,Mn}$ values were indicated by a negligible difference between the initial and final $I_{L,Fc}$ currents. This procedure led to the following values of R_{lim} (= $(I_{L,Mn}/I_{L,Fc})(c_{Fc}/c_{Mn}) = n_{app}D_{Mn}/D_{Fc}$):[24] $R_{lim}(S_a)$ = 1.05; $R_{lim}(S_b)$ = 1.06; $R_{lim}(S_c)$ = 0.41; $R_{lim}(S_d)$ = 0.98.

Extraction of the n_{app} and D values from the combined expressions for R_{chrono} and R_{lim}[24] gave (a) for the reduction of [Mn(Br)(CO)$_3$(iPr-DAB)] in THF (S_a), n_{app} = 1.92 ± 0.08 and $D_{Mn} = (0.55 \pm 0.02)D_{Fc}$; (b) for the reduction of [Mn(Br)(CO)$_3$-(iPr-DAB)] in MeCN (S_b), n_{app} = 1.96 ± 0.08 and $D_{Mn} = (0.54 \pm 0.02)D_{Fc}$; (c) for the reduction of [Mn(THF)(CO)$_3$(iPr-DAB)]$^+$ in THF (S_c), $n_{app} = 0.85 \pm 0.15$ and $D_{Mn} = (0.48 \pm 0.07)D_{Fc}$; (d) for the reduction of [Mn(MeCN)(CO)$_3$(iPr-DAB)]$^+$ in MeCN (S_d) $n_{app} = 1.86 \pm 0.10$ and $D_{Mn} = (0.55 \pm 0.06)D_{Fc}$.

Using the known D_{Fc} values in THF (8.0×10^{-6} cm^2 s^{-1}) and MeCN (1.9×10^{-5} cm^2 s^{-1})[24] gives, for example, D_{Mn} ([Mn-(Br)(CO)$_3$(iPr-DAB)]) = 4.4×10^{-6} (in THF) and 1.03×10^{-5} (in MeCN) cm^2 s^{-1}. The characteristic time for the steady-state measurement[22] is then $T_c = r_o^2/D$ = 227 (in THF) or 97 ms (in MeCN), which indeed falls within the range $T_c = \theta$ = 50−300 ms chosen for the chronoamperometric measurements with the 500 μm Pt disk, thus validating the determined values of n_{app} and D_{Mn}. The value θ = 227 ms corresponds to the CV scan rate v = 110 mV/s. This result implies that the reduction of [Mn(Br)(CO)$_3$(iPr-DAB)] in THF at the voltammetric scan rate v = 100 mV/s corresponds to a two-electron process (see eqs 1−3).

Results

IR and UV−Vis Spectroelectrochemistry. In the following sections, the spectroscopic changes accompanying reduction of the complexes [Mn(X)(CO)$_3$(iPr-DAB)]^n (n = 0, X = Otf, Br, Me, Bz; n = +1, X = nPrCN, P(OMe)$_3$) will be described. All measurements were carried out in nPrCN, unless stated otherwise. Table 1 summarizes the IR ν(CO) wavenumbers and UV−vis absorption maxima of all complexes under study and their reduction products.[25] The redox potentials are listed in Table 2.

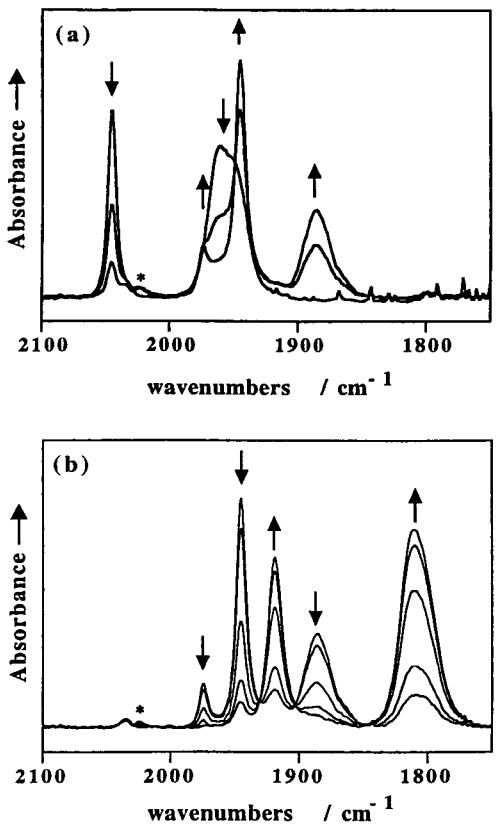

Figure 2. IR spectral changes in the ν(CO) region during the reduction of [Mn(nPrCN)(CO)$_3$(iPr-DAB)]$^+$. (a) The initial reduction step producing the dimer [Mn(CO)$_3$(iPr-DAB)]$_2$. (b) The subsequent reduction step producing the anion [Mn(CO)$_3$(iPr-DAB)]$^-$. The asterisk denotes a small amount of a side product P_1 (see text). Conditions: T = 293 K, in nPrCN, electrolysis in a room temperature OTTLE cell.[19]

[Mn(X)(CO)$_3$(iPr-DAB)]$^+$ (X = nPrCN, P(OMe)$_3$). Dissolving [Mn(Otf)(CO)$_3$(iPr-DAB)] in nPrCN at room temperature resulted in rapid substitution of the weakly bound triflate anion by a solvent molecule. Reduction of [Mn(nPrCN)(CO)$_3$(iPr-DAB)]$^+$ within the OTTLE cell yielded a single product, which exhibited ν(CO) bands at 1975(w), 1945 (vs), and 1886 (m,br) cm^{-1} (Figure 2a). Five new ν(CO) bands were found in a better-resolved IR spectrum of this species in THF (see Table 1). The reduction led to disappearance of the Mn−diimine

(25) The average C═O force constants k_{av}[26] of these species in Table 1 were calculated using eq 5. Exact determination of all four CO force constants, k_{ax}, k_{eq}, $k_{ax,eq}$, $k_{eq,eq}$, by the Cotton−Kraihanzel energy factored force field method[27,28] was impossible due to the lack of the wavenumbers of the ^{13}CO-enriched positional isotopomers. The empirical method of Timney[29] was also not applied as the exact geometry of the five-coordinate reduced complexes was unknown. Equation 5: $k_{av} = 4.0383 \times 10^{-4} (\Sigma_i g_i \nu_i^2)/(\Sigma_i g_i)$, where g_i = degeneracy of the ith CO stretching mode of the frequency ν_i (in cm^{-1}).

(26) Braterman, P. S. *Metal Carbonyl Spectra*; Academic Press: London, 1975.

(27) Turner, J. J.; Grevels, F. W.; Howdle, S. M.; Jacke, J.; Haward, M. T.; Klotzbücher, W. E. *J. Am. Chem. Soc.* **1991**, *113*, 8347.

(28) (a) Kraihanzel, C. S.; Cotton, F. A. *Inorg. Chem.* **1963**, *2*, 533. (b) Cotton, F. A.; Kraihanzel, C. S. *J. Am. Chem. Soc.* **1962**, *84*, 4432.

(29) Timney, J. A. *Inorg. Chem.* **1979**, *18*, 2502.

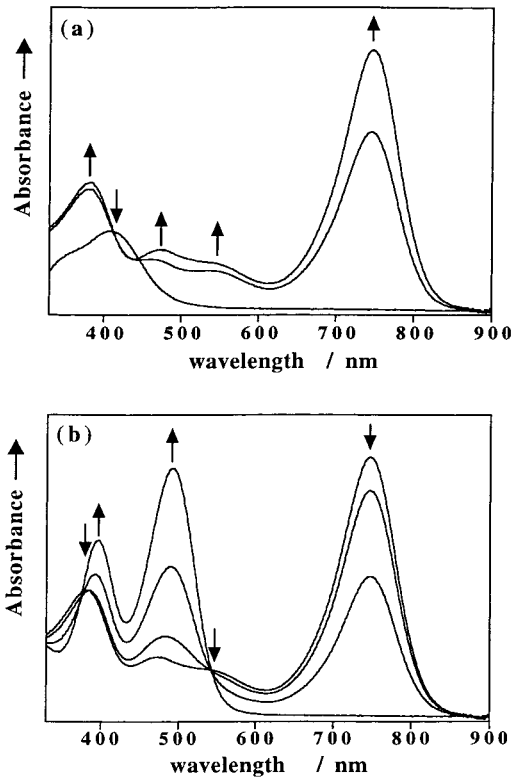

Figure 3. UV−vis spectral changes in the visible region during the reduction of [Mn(nPrCN)(CO)$_3$(iPr-DAB)]$^+$. (a) The initial reduction step producing the dimer [Mn(CO)$_3$(iPr-DAB)]$_2$. (b) The subsequent reduction step producing the anion [Mn(CO)$_3$(iPr-DAB)]$^-$. Conditions: see Figure 1.

charge transfer (MLCT, metal-to-ligand charge transfer)[4] absorption band of [Mn(nPrCN)(CO)$_3$(iPr-DAB)]$^+$ at 405 nm and to the rise of an intense absorption band at 744 nm and smaller bands at 550, 480, and 370 nm (see Figure 3a). These IR and UV−vis features point to the formation of the stable metal−metal-bonded dimer [Mn(CO)$_3$(iPr-DAB)]$_2$.[10,11c] Like [Mn(CO)$_3$(bpy)]$_2$[12,13] and [Ru(Me)(CO)$_2$(iPr-DAB)]$_2$,[30] [Mn(CO)$_3$(iPr-DAB)]$_2$ also possesses an eclipsed conformation (C_{2v} point group) in solution. Apart from this dimer, ν(CO) bands of a minor unassigned species P_1 were detected in the IR spectrum (see Figure 2a and Table 1). Subsequent reduction of the dimer [Mn(CO)$_3$(iPr-DAB)]$_2$ gave rise to two strong ν(CO) bands at 1919 and 1811 (br) cm^{-1} (Figure 2b) which belong to the stable five-coordinate anion [Mn(CO)$_3$(iPr-DAB)]$^-$. This assignment is in line with the similar ν(CO) wavenumbers of [Mn(CO)$_3$(bpy)]$^-$.[4,13] Related anions are typically formed on two-electron reduction of [Ru(X)(R)(CO)$_2$(α-diimine)][20,30,31] and [Re(X)(CO)$_3$(α-diimine)][3a,b,d,17] (X = halide, R = alkyl) containing basic α-diimine ligands. The origin of the visible absorption of [Mn(CO)$_3$(iPr-DAB)]$^-$ (see Figure 3b and Table 1) is discussed below. Reoxidation of [Mn(CO)$_3$(iPr-DAB)]$^-$ in nPrCN at 293 K only yielded the dimer [Mn(CO)$_3$(iPr-DAB)]$_2$. [Mn(nPrCN)(CO)$_3$(iPr-DAB)]$^+$ was ultimately recovered on the subsequent oxidation of the dimer at a more positive potential (see Table 2).

The OTTLE experiment with [Mn(nPrCN)(CO)$_3$(iPr-DAB)]$^+$ was also carried out at 198 K in nPrCN. The reduction directly yielded the two-electron-reduced anion [Mn(CO)$_3$(iPr-DAB)]$^-$. The dimer [Mn(CO)$_3$(iPr-DAB)]$_2$ was only produced at a very low concentration (see Figure 4, Supporting Information). No additional ν(CO) bands were observed, which might indicate formation of 18-electron radicals [Mn(nPrCN)(CO)$_3$(iPr-DAB)]$^\bullet$.

The cation [Mn(nPrCN)(CO)$_3$(iPr-DAB)]$^+$ was also reduced at room temperature in the presence of a 200-fold excess of PPh$_3$. The large excess of PPh$_3$ had, however, no effect on the quantitative yield of the dimer [Mn(CO)$_3$(iPr-DAB)]$_2$. This result demonstrates that PPh$_3$, similarly to nPrCN, does not stabilize the transient radical [Mn(CO)$_3$(iPr-DAB)]$^\bullet$ (see below) in the course of the cathodic process.

In the presence of 1 equiv of P(OMe)$_3$, [Mn(nPrCN)(CO)$_3$(iPr-DAB)]$^+$ first converted *via* an electrode-catalyzed reaction[3a] into [Mn{P(OMe)$_3$}(CO)$_3$(iPr-DAB)]$^+$ (see Table 1). In the presence of a 200-fold excess of P(OMe)$_3$, [Mn{P(OMe)$_3$}(CO)$_3$(iPr-DAB)]$^+$ was only observed as a transient species. The electrode-catalyzed reaction then ultimately gave the dicarbonyl derivative [Mn{P(OMe)$_3$}$_2$(CO)$_2$(iPr-DAB)]$^+$ (see Table 1). Subsequent reduction of the latter cation was accompanied by secondary chemical and electron-transfer reactions that mainly produced the anion [Mn(CO)$_3$(iPr-DAB)]$^-$ and was not further investigated. The cations [Mn{P(OMe)$_3$}(CO)$_3$(iPr-DAB)]$^+$ remained stable at 183−198 K. Their reduction then yielded the 18e radicals [Mn{P(OMe)$_3$}(CO)$_3$(iPr-DAB)]$^\bullet$ (see Table 1), concomitantly with a small amount of [Mn(CO)$_3$(iPr-DAB)]$^-$. This result indicates that [Mn{P(OMe)$_3$}(CO)$_3$(iPr-DAB)]$^\bullet$ slowly lose P(OMe)$_3$ to give the five-coordinate radicals [Mn(CO)$_3$(iPr-DAB)]$^\bullet$, which are further reducible at the reduction potential of [Mn{P(OMe)$_3$}(CO)$_3$(iPr-DAB)]$^+$. This assumption was corroborated by the cyclic voltammetric results (see below). Subsequent reduction of [Mn{P(OMe)$_3$}(CO)$_3$(iPr-DAB)]$^\bullet$ led to complete dissociation of the P(OMe)$_3$ ligand, producing [Mn(CO)$_3$(iPr-DAB)]$^-$. Notably, reoxidation of the five-coordinate anion in the presence of P(OMe)$_3$ led *directly* to the recovery of the parent cation [Mn{P(OMe)$_3$}(CO)$_3$(iPr-DAB)]$^+$.

[Mn(Br)(CO)$_3$(iPr-DAB)]. According to the IR and UV−vis OTTLE results, reduction of [Mn(Br)(CO)$_3$(iPr-DAB)] at room temperature *simultaneously* afforded both the dimer [Mn(CO)$_3$(iPr-DAB)]$_2$ and the anion [Mn(CO)$_3$(iPr-DAB)]$^-$. Reoxidation of the ultimate reduction product [Mn(CO)$_3$(iPr-DAB)]$^-$ *simultaneously* produced both [Mn(Br)(CO)$_3$(iPr-DAB)] and the dimer [Mn(CO)$_3$(iPr-DAB)]$_2$. This observation implies that the conversion of [Mn(Br)(CO)$_3$(iPr-DAB)] into [Mn(CO)$_3$(iPr-DAB)]$^-$ on the reduction and *vice versa* on the reoxidation does not pass *via* the intermediate [Mn(CO)$_3$(iPr-DAB)]$_2$. Unambigous evidence for this mechanistic assumption was gained from the cyclic voltammetric studies (see below).

Finally, the starting complex [Mn(Br)(CO)$_3$(iPr-DAB)] was completely recovered on subsequent oxidation of [Mn(CO)$_3$(iPr-DAB)]$_2$ at more positive potentials (see Table 2) due to the rapid recoordination of Br$^-$ present in the thin solution layer.

[Mn(X)(CO)$_3$(iPr-DAB)] (X = Me, Bz). Reduction of [Mn(X)(CO)$_3$(iPr-DAB)] (X = Me, Bz) at room temperature, monitored by IR and UV−vis spectroscopies,

(30) tom Dieck, H.; Rohde, W.; Behrens, U. *Z. Naturforsch.* **1989**, *44B*, 158.
(31) (a) Nieuwenhuis, H. A.; Hartl, F.; Stufkens, D. J. Unpublished results. (b) Nieuwenhuis, H. A. Ph.D. Thesis, University of Amsterdam, Amsterdam, The Netherlands, 1994.

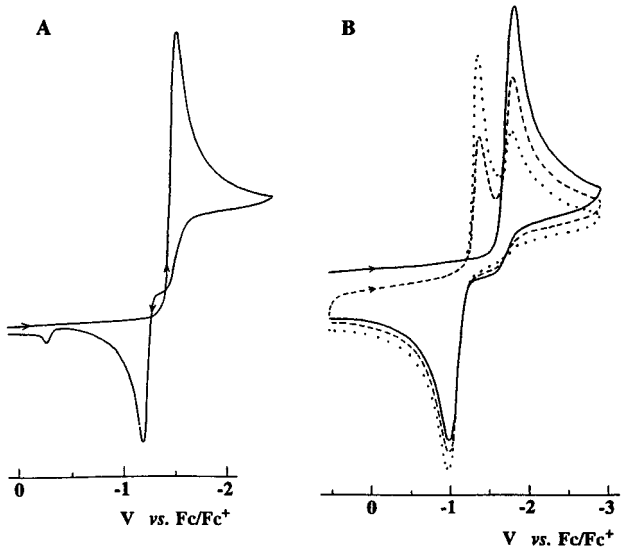

Figure 5. Cyclic voltammogram of [Mn(Br)(CO)$_3$(iPr-DAB)] in MeCN at T = 293 K, recorded with a Pt disk electrode (500 μm diameter). (A) ν = 100 mV/s. (B) ν = 20 V/s (full line = first cycle; dashed line = first repeated scan; dotted line = eighth repeated scan).

directly afforded the anion [Mn(CO)$_3$(iPr-DAB)]$^-$ (see Table 1). Reoxidation of the anion produced, in this case, a carbonyl species with strong ν(CO) bands at 2023, 1934, and 1919 cm^{-1} (for X = Bz) and at 2023 and 1923 (br) cm^{-1} (for X = Me). These wavenumbers closely resemble those of the as yet unidentified product P$_1$, as well as those of neutral [Mn(Br)(CO)$_3$(iPr-DAB)] (see Table 1). Formation of the dimer [Mn(CO)$_3$(iPr-DAB)]$_2$ was not observed. Reduction of [Mn(Bz)(CO)$_3$-(iPr-DAB)] at 198 K yielded two products in nearly equal concentration, *viz.* the anion [Mn(CO)$_3$(iPr-DAB)]$^-$ and a tricarbonyl complex with ν(CO) bands at 1985, 1882, and 1873 cm^{-1}. The latter product was thermally unstable. The reduction of [Mn(Me)(CO)$_3$(iPr-DAB)] at 198 K yielded [Mn(CO)$_3$(iPr-DAB)]$^-$ only as a minor product. Further experiments need to be performed in this area.

Cyclic Voltammetry. [Mn(X)CO$_3$(iPr-DAB)]^n (n = 0, X = Br; n = +1, X = MeCN, THF). The cyclic voltammograms of the complexes [Mn(Br)(CO)$_3$(iPr-DAB)], in MeCN and THF, [Mn(MeCN)(CO)$_3$(iPr-DAB)]$^+$, and [Mn(THF)(CO)$_3$(iPr-DAB)]$^+$ are depicted in Figures 5A,B, 6 (Supporting Information), 7A,B (7B in Supporting Information), and 8, respectively.

Reduction Paths. The cyclic voltammogram of the complex [Mn(Br)(CO)$_3$(iPrDAB)] in MeCN at ν = 100 mV/s shows a single cathodic peak at $E_{p,c}$ = −1.57 V (Figure 5A), which corresponds to the total transfer of two electrons (n_{app} = 1.95). The predominant π*(iPr-DAB) character of the LUMO of [Mn(Br)(CO)$_3$(iPr-DAB)][5] implies that the reduction initially affords the radical anion [Mn(Br)(CO)$_3$(iPr-DAB)]$^{\bullet-}$, which rapidly loses the Br$^-$ ligand and converts to the coordinatively unsaturated radical [Mn(CO)$_3$(iPr-DAB)]$^\bullet$. This transient species is then instantaneously reduced with the second electron, resulting in the formation of the five-coordinate anion [Mn(CO)$_3$(iPr-DAB)]$^-$. Importantly, we have independently proved that the two-electron-reduced anion [Mn(CO)$_3$(iPr-DAB)]$^-$ reacts smoothly with an equivalent amount of [Mn(Br)(CO)$_3$(iPr-DAB)] to give the dimer [Mn(CO)$_3$(iPr-DAB)]$_2$ as the single

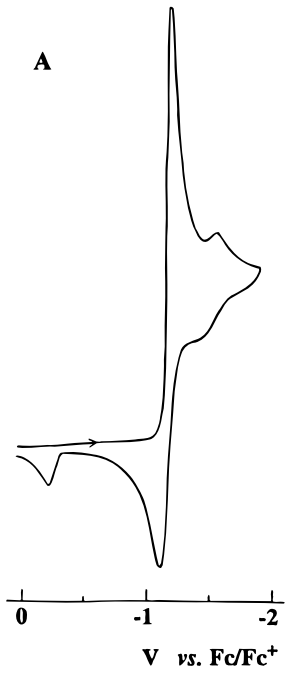

Figure 7. (A) Cyclic voltammogram of [Mn(MeCN)(CO)$_3$-(iPr-DAB)]$^+$ in MeCN at T = 293 K, recorded with a Pt disk electrode (500 μm diameter) at ν = 100 mV/s.

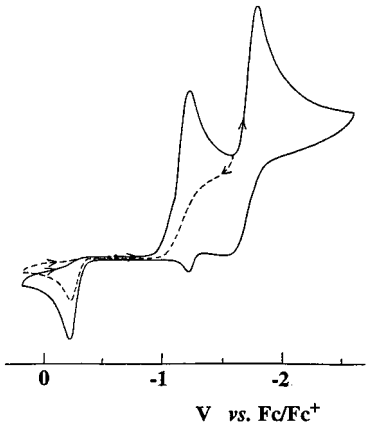

Figure 8. Cyclic voltammogram of [Mn(THF)(CO)$_3$(iPr-DAB)]$^+$ in THF at T = 293 K, recorded with a Pt disk electrode (500 μm diameter) at ν = 100 mV/s.

product. There was, however, no evidence to suggest the presence of the dimer [Mn(CO)$_3$(iPr-DAB)]$_2$ on the time scale defined by scan rates $\nu \geq$ 50 mV/s. Simultaneous formation of [Mn(CO)$_3$(iPr-DAB)]$^-$ and the dimer was nevertheless confirmed by the corresponding spectroelectrochemical experiments on the seconds time scale (see above). [Mn(CO)$_3$(iPr-DAB)]$^-$ is thus formed *via* the ECE sequence as described by eqs 1−3 and summarized in Scheme 1. An alternative route to this anion might be the DISP 1 sequence defined by eqs 6 and 7. Revealing evidence against the disproportionation route of [Mn(Br)(CO)$_3$(iPr-DAB)]$^{\bullet-}$ is the crossed voltammetric response in Figures 5A and 6. This characteristic feature is in fact equivalent to a hump on the corresponding chronoamperometric anodic current trace, crossing the line of zero current, which is claimed for the ECE sequence but never for the DISP 1 path.[32] We assume that the ECE mechanism is favored

(32) Amatore, C.; Savéant, J. M. *J. Electroanal. Chem., Interfacial Electrochem.* **1980**, *107*, 353.

Scheme 1

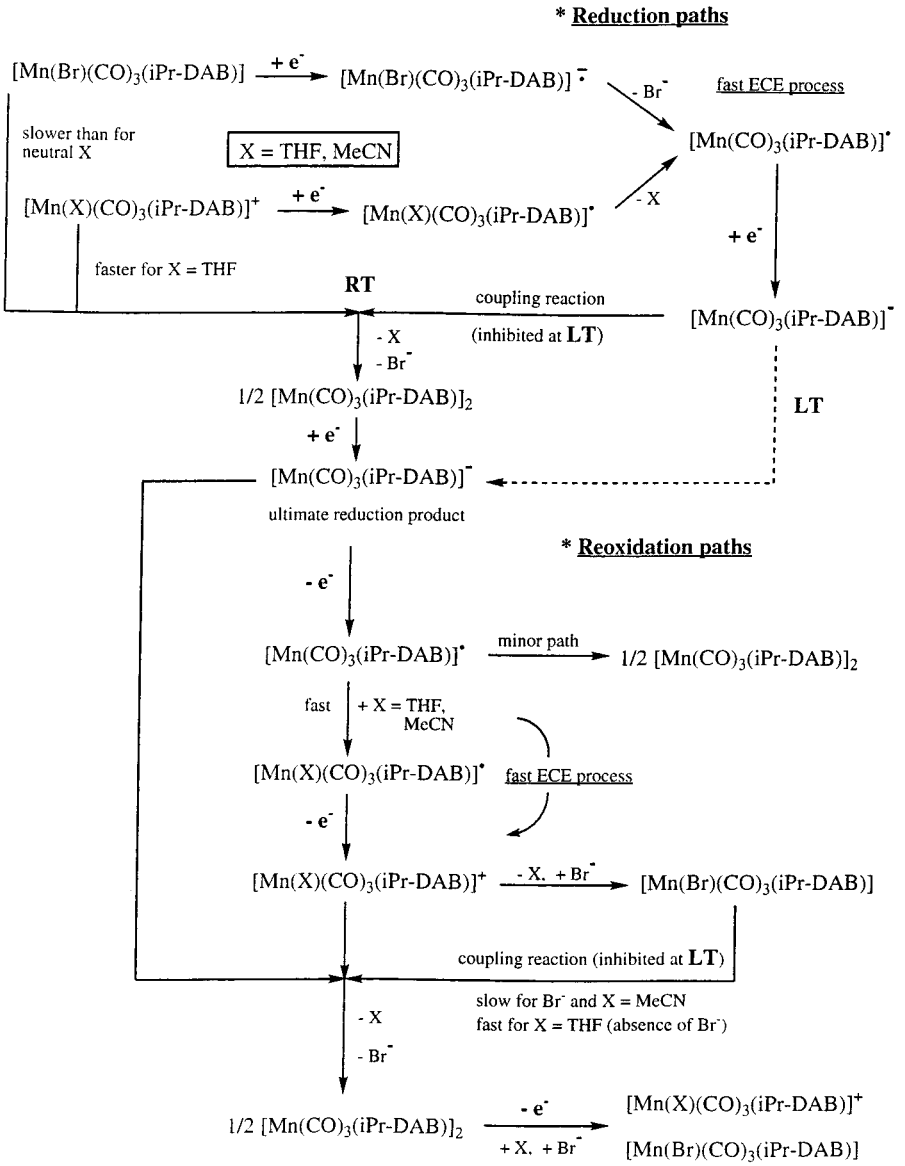

by very fast dissociation of the Br^- ligand from the radical anion $[Mn(Br)(CO)_3(iPr\text{-}DAB)]^{\bullet -}$ (see eq 2) *prior* to its diffusion into the bulk solution, which permits further reduction of the transient radical $[Mn(CO)_3(iPr\text{-}DAB)]^{\bullet}$ still at the electrode surface. Reoxidation of

$$[Mn(Br)(CO)_3(iPr\text{-}DAB)]^{\bullet -} + [Mn(CO)_3(iPr\text{-}DAB)]^{\bullet} \rightarrow [Mn(Br)(CO)_3(iPr\text{-}DAB)] + [Mn(CO)_3(iPr\text{-}DAB)]^{-} \quad (6)$$

$$[Mn(X)(CO)_3(iPr\text{-}DAB)]^{\bullet} + [Mn(CO)_3(iPr\text{-}DAB)]^{\bullet} \rightarrow (X = THF, MeCN)$$
$$[Mn(X)(CO)_3(iPr\text{-}DAB)]^{+} + [Mn(CO)_3(iPr\text{-}DAB)]^{-} \quad (7)$$

$[Mn(Br)(CO)_3(iPr\text{-}DAB)]^{\bullet -}$ could not, indeed, be observed even at $v = 4 \times 10^5$ V/s, which allows an estimation[33] of the lower limit of the cleavage rate constant of $[Mn(Br)(CO)_3(iPr\text{-}DAB)]^{\bullet -}$: $k >> 10^7$ s^{-1}. The upper limit is obviously $k < \boldsymbol{k}T/h = 10^{12}$ s^{-1} ($\boldsymbol{k}$ = Boltzmann constant).

For the reduction of $[Mn(Br)(CO)_3(iPr\text{-}DAB)]$ in MeCN, the scan rate dependence of the cathodic-peak potential, $\delta E_{p,c}/\delta \log(v)$, is a straight line with a slope of −30 mV decade^{-1} within the interval $v = 0.1$−2.0 V/s (see Figure 9a). This value characterizes a monomolecular E_rC_i mechanism[35] represented herein by eqs 1 and 2, implying that the dissociation of Br^- from $[Mn(Br)(CO)_3(iPr\text{-}DAB)]^{\bullet -}$ is the rate-determining step in the ECE reduction path of $[Mn(Br)(CO)_3(iPr\text{-}DAB)]$ in Scheme 1. The electron transfer becomes irreversible for $v > 2$ V/s, which corresponds to the observed slope of −60 mV decade^{-1} (see Figure 9a). The normalized cathodic

(33) For an E_rC_i mechanism, a cyclic voltammetric response to an electron transfer step remains chemically totally irreversible at a particular scan rate v provided[34] the follow-up rate constant $k >> 10/\tau$, where $\tau = \Delta E_p \cdot v^{-1}$ and $\Delta E_p = E_{p,c} + E_{p,a} - 2E_\lambda$ (E_λ is the switching potential, *ca.* 300 mV behind the $E_{p,c}$ value). In our case, $v = 4 \times 10^5$ V/s, hence $k >> 10\ (v/\Delta E_p) = 7 \times 10^6$ s^{-1} ($\sim 10^7$ s^{-1}).

(34) Nicholson, R. S.; Shain, I. *Anal. Chem.* **1964**, *36*, 704.

(35) Bard, A. J.; Faulkner, L. R. *Electrochemical Methods, Fundamentals and Applications*; Wiley & Sons: New York, 1980; Chapter 11.

current $I_p v^{-1/2}$ remains fairly constant at the moderate scan rates where the E_rC_i mechanism applies. This result is in line with the hindered coupling reaction between $[Mn(CO)_3(iPr\text{-}DAB)]^-$ and $[Mn(Br)(CO)_3(iPr\text{-}DAB)$, corresponding to eq 4, on this time scale.

Considering the $E_rC_i(E)$ reduction path of $[Mn(Br)(CO)_3(iPr\text{-}DAB)]$, the known relationship[35] between $E_{p,c}$, $E_{1/2}$, the scan rate v, and the cleavage rate constant k with the above k limits predicts that the $E_{1/2}$ value of the redox couple $[Mn(Br)(CO)_3(iPr\text{-}DAB)]^{0/\bullet-}$ lies in the interval $-1.85\ V < E_{1/2} < -1.71\ V$ *vs* Fc/Fc^+, *i.e.*, much more negatively than $E_{1/2}$ of the redox couple $[Mn(CO)_3(iPr\text{-}DAB)]^{\bullet/-}$ (see below). From this comparison, it is thus obvious that the five-coordinate radicals $[Mn(CO)_3(iPr\text{-}DAB)]^\bullet$ have to be reduced instantaneously to the corresponding anions at the reduction potential of parent $[Mn(Br)(CO)_3(iPr\text{-}DAB)]$. Their consecutive dimerization to $[Mn(CO)_3(iPr\text{-}DAB)]_2$, therefore, cannot compete[16] with this cathodic step, as shown in Scheme 1; instead, the dimer is only formed *via* the coupling reaction following eq 4.

The same two-electron reduction path can be drawn for the reduction of the cations $[Mn(X)(CO)_3(iPr\text{-}DAB)]^+$ (X = MeCN, THF), where the transient $[Mn(CO)_3(iPr\text{-}DAB)]^\bullet$ originates from the unstable radicals $[Mn(X)(CO)_3(iPr\text{-}DAB)]^\bullet$ (see Scheme 1). Notably, the cyclic voltammogram of $[Mn(MeCN)(CO)_3(iPr\text{-}DAB)]^+$ at room temperature and $v = 100$ mV/s (Figure 7A) shows an additional, small cathodic peak at $E_{p,c} = -1.64$ V due to the reduction of $[Mn(CO)_3(iPr\text{-}DAB)]_2$, in agreement with $n_{app} = 1.86$.[36] This cathodic peak becomes diminished on increasing the scan rate (see Figure 7B), as the zero-electron coupling reaction between $[Mn(CO)_3(iPr\text{-}DAB)]^-$ and parent $[Mn(MeCN)(CO)_3(iPr\text{-}DAB)]^+$ is too slow to produce a detectable amount of $[Mn(CO)_3(iPr\text{-}DAB)]_2$ at $v \geq 2$ V/s. On the OTTLE time scale of 10^1-10^2 s, however, only $[Mn(CO)_3(iPr\text{-}DAB)]_2$ is produced in this case (see above).

On the other hand, the well-developed cathodic peak of $[Mn(CO)_3(iPr\text{-}DAB)]_2$ at $E_{p,c} = -1.73$ V for $v = 100$ mV/s (see Figure 8) shows that $[Mn(THF)(CO)_3(iPr\text{-}DAB)]^+$ reacts with the anion $[Mn(CO)_3(iPr\text{-}DAB)]^-$ considerably more rapidly than the MeCN- and, in particular, Br-derivatives (see Scheme 1). The reduction of the cation at $E_{p,c} = -1.19$ V then corresponds to the total transfer of one electron, in agreement with experimentally determined $n_{app} = 0.85 \pm 0.15$. The above coupling reaction becomes less competitive on increasing the scan rate to $v = 2$ V/s, where $\delta E_{p,c}/\delta \log(v) = -30$ mVdecade^{-1} still applies, which is reflected in the slightly increasing function $\delta(I_p v^{-1/2})/\delta \log(v)$ due to $n_{app} > 1$, see Figure 9b.

Reoxidation Paths. Oxidation of $[Mn(CO)_3(iPr\text{-}DAB)]^-$ ($E_{p,a}$ in Table 2, see Figures 5−8) produces, at room temperature, the radicals $[Mn(CO)_3(iPr\text{-}DAB)]^\bullet$. Cyclic voltammograms of parent $[Mn(Br)(CO)_3(iPr\text{-}DAB)]$ (Figures 5A and 6) show that these radicals do not concomitantly dimerize, as the detectable amount of $[Mn(CO)_3(iPr\text{-}DAB)]_2$ (oxidized at $E_{p,a} = -0.24$ V) is rather small in MeCN on the time scale defined by $v = 100$ mV/s and only slightly larger in THF. Scan reversal beyond the anodic peak of $[Mn(CO)_3(iPr\text{-}DAB)]^-$ in MeCN reveals a new cathodic peak at −1.26 V due to the reduction of $[Mn(MeCN)(CO)_3(iPr\text{-}DAB)]^+$, whose peak current considerably increases at higher scan rates and on repeated scans (see Figure 5B). Apparently, the radicals $[Mn(CO)_3(iPr\text{-}DAB)]^\bullet$ preferably take up the solvent molecules and convert to $[Mn(MeCN)(CO)_3(iPr\text{-}DAB)]^\bullet$, which instantaneously oxidize at the applied oxidation potential of $[Mn(CO)_3(iPr\text{-}DAB)]^-$ (see Table 2) to the corresponding cations detectable on the reverse cathodic scan (see Scheme 1). This $E_rC_i(E)$ sequence, where the rate-determining step is the pseudo-first-order chemical reaction of $[Mn(CO)_3(iPr\text{-}DAB)]^\bullet$ with the MeCN solvent, was unequivocally confirmed by the scan-rate dependence of the $E_{p,a}$ potential of $[Mn(CO)_3(iPr\text{-}DAB)]^-$: $\delta E_{p,a}/\delta \log(v) = 30$ mV decade^{-1} for $v = 0.05-2$ V/s.[37] For the consecutive dimerization of $[Mn(CO)_3(iPr\text{-}DAB)]^\bullet$ as a second-order reaction, $\delta E_{p,a}/\delta \log(v) = 20$ mVdecade^{-1} should be observed.[35] The same situation applies for the oxidation of $[Mn(CO)_3(iPr\text{-}DAB)]^-$ in THF which produces $[Mn(THF)(CO)_3(iPr\text{-}DAB)]^+$. The detection of the latter cations on the reverse cathodic scan, however, demands considerably higher scan rates relative to the detection limit for $[Mn(MeCN)(CO)_3(iPr\text{-}DAB)]^+$, *viz.* $v = 500$ V/s *vs* 0.1 V/s at room temperature, respectively. The spectroelectrochemical experiments have shown that the solvent ligand X in $[Mn(X)(CO)_3(iPr\text{-}DAB)]^+$ becomes readily substituted by the Br^- anions liberated on reduction of $[Mn(Br)(CO)_3(iPr\text{-}DAB)]$. This substitution reaction is faster for X = THF than that for X = MeCN. It leads to the recovery of parent $[Mn(Br)(CO)_3(iPr\text{-}DAB)]$ whose subsequent zero-electron-coupling reaction with non-oxidized $[Mn(CO)_3(iPr\text{-}DAB)]^-$ to give $[Mn(CO)_3(iPr\text{-}DAB)]_2$ (see Scheme 1) is rather slow relative to that of $[Mn(X)(CO)_3(iPr\text{-}DAB)]^+$ (X = THF, MeCN) and is hardly observable on the time scale of cyclic voltammetry defined by $v \geq 50$ mV/s. This implies that the corresponding reaction rate constant must be less than a few hundred $M^{-1}\ s^{-1}$.[34] The higher stability of $[Mn(Br)(CO)_3(iPr\text{-}DAB)]$ toward the nucleophilic attack of $[Mn(CO)_3(iPr\text{-}DAB)]^-$ then explains the simultaneous IR OTTLE detection of $[Mn(CO)_3(iPr\text{-}DAB)]_2$ and $[Mn(Br)(CO)_3(iPr\text{-}DAB)]$ during the oxidation of $[Mn(CO)_3(iPr\text{-}DAB)]^-$ produced from $[Mn(Br)(CO)_3(iPr\text{-}DAB)]$ at room temperature and on the other hand, the exclusive formation of $[Mn(CO)_3(iPr\text{-}DAB)]_2$ in the absence of uncoordinated Br^- (see above).

$[Mn\{P(OMe)_3\}(CO)_3(iPr\text{-}DAB)]^+$. The cyclic voltammogram of the cation $[Mn\{P(OMe)_3\}(CO)_3(iPr\text{-}DAB)]^+$ in nPrCN at 223 K showed a chemically reversible cathodic process at $E_{p,c} = -1.36$ V due to the formation of $[Mn\{P(OMe)_3\}(CO)_3(iPr\text{-}DAB)]^\bullet$. This radical complex is not completely stable at room temperature. In the spectroelectrochemical section, we have documented that $T \approx 190$ K was needed to stabilize $[Mn\{P(OMe)_3\}(CO)_3(iPr\text{-}DAB)]^\bullet$ on the time scale of minutes. The subsequent reduction of $[Mn\{P(OMe)_3\}(CO)_3(iPr\text{-}DAB)]^\bullet$ was found at $E_{p,c} = -2.38$ V. This cathodic step was chemically irreversible and produced $[Mn(CO)_3(iPr\text{-}DAB)]^-$, as indicated the by the appearance of its anodic

(36) This assignment also corresponds with thin-layer cyclic voltammograms recorded in the course of the corresponding OTTLE experiments.

(37) Following the E_rC_i mechanism, the observed positive $E_{p,a}$ ($[Mn(CO)_3(iPr\text{-}DAB)]^-$) shift is directed toward the $E_{1/2}$ potential of the reversible couple $[Mn(CO)_3(iPr\text{-}DAB)]^{\bullet/-}$.[35] The five-coordinate radical $[Mn(CO)_3(iPr\text{-}DAB)]^\bullet$ thus reduces significantly more positively then $[Mn(X)(CO)_3(iPr\text{-}DAB)]^n$ ($n = 0$, X = Br; $n = +1$, X = MeCN, THF), as considered in the description of the reduction paths of the latter complexes.

Scheme 2

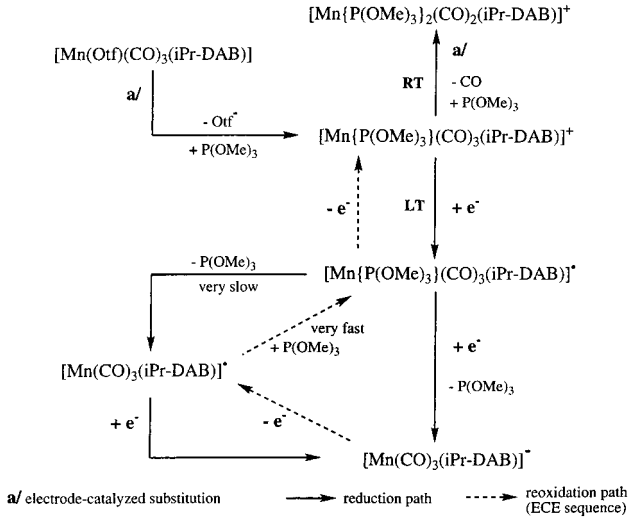

peak at $E_{p,a} = -1.20$ V (see Table 2) on the reverse scan. Addition of excess $P(OMe)_3$ into the solution of [Mn{$P(OMe)_3$}$(CO)_3$(iPr-DAB)]$^+$ at room temperature resulted in a significant decrease of the peak at $E_{p,c} = -1.36$ V in favor of a new cathodic peak at $E_{p,c} = -1.66$ V attributed to the reduction of the dicarbonyl cation [Mn{$P(OMe)_3$}$_2(CO)_2$(iPr-DAB)]$^+$. In line with the spectroelectrochemical experiments, this electrocatalytic[38] reaction became completely inhibited at 223 K.

Importantly, there was no evidence for the formation of the dimer [Mn$(CO)_3$(iPr-DAB)]$_2$ ($E_{p,a} = -0.24$ V) on the reoxidation of [Mn$(CO)_3$(iPr-DAB)]$^-$ in the presence of excess $P(OMe)_3$, which also agrees with the above OTTLE results.

On the basis of the combined spectroelectrochemical/cyclic voltammetric evidence, the redox cycle of [Mn{$P(OMe)_3$}$(CO)_3$(iPr-DAB)]$^+$ is summarized in Scheme 2.

[Mn(X)(CO)$_3$(iPr-DAB)] (X = Me, Bz). The complex [Mn(Bz)$(CO)_3$(iPr-DAB)] is reduced slightly more positively than the derivative with the more electron-releasing Me group (see Table 2).[39] Scan reversal beyond the cathodic peaks of [Mn(Me)$(CO)_3$(iPr-DAB)] and [Mn(Bz)$(CO)_3$(iPr-DAB)] showed an anodic peak at $E_{p,a} = -1.22$ V belonging to the oxidation of [Mn$(CO)_3$(iPr-DAB)]$^-$. Identical with [Mn(Br)$(CO)_3$(iPr-DAB)], the Me derivative initially undergoes a one-electron reduction which gives the corresponding radical anion (eq 8). [Mn(Me)$(CO)_3$(iPr-DAB)]$^{\bullet -}$ is however, considerably more stable than [Mn((Br)$CO)_3$(iPr-DAB)]$^{\bullet -}$, as its reoxidation could still be observed on the reverse anodic scan (see Figure 10).

$$[Mn(Me)(CO)_3(iPr\text{-}DAB)] + e^- \rightleftharpoons [Mn(Me)(CO)_3(iPr\text{-}DAB)]^{\bullet -} \quad (8)$$

In contrast to the two-electron (ECE) reduction path of [Mn(Br)$(CO)_3$(iPr-DAB)] (see Scheme 1), we assume that the secondary chemical reaction of the radical anion [Mn(Me)$(CO)_3$(iPr-DAB)]$^{\bullet -}$ directly produces the anion [Mn$(CO)_3$(iPr-DAB)]$^-$ as the only carbonyl species detected during the corresponding IR OTTLE experiment at room temperature and the radical Me$^\bullet$ whose fate was not studied (eq 9). Recall that the spectroscopic properties of the related stable radical anions [Re(X)$(CO)_3$(iPr-DAB)]$^{\bullet -}$ (X = Me, Et, Bz) point to the anionic chromophore Re$(CO)_3$(iPr-DAB)$^-$ with the bound X$^\bullet$ ligand.[17]

$$[Mn(Me)(CO)_3(iPr\text{-}DAB)]^{\bullet -} \rightarrow [Mn(CO)_3(iPr\text{-}DAB)]^- + Me^\bullet \quad (9)$$

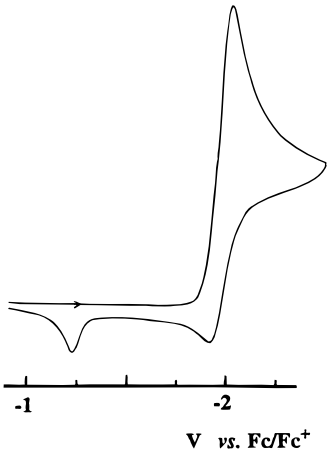

Figure 10. Cyclic voltammogram of [Mn(Me)$(CO)_3$(iPr-DAB)] in nPrCN at $T = 293$ K, recorded with a freshly repolished Pt disk electrode (500 μm diameter) at $\nu = 100$ mV/s.

Notably, both complexes [Mn(X)$(CO)_3$(iPr-DAB)] (X = Me, Bz) are oxidized significantly more negatively than [Mn(Br)$(CO)_3$(iPr-DAB)] (see Table 2). According to a DFT-MO study[5] of the model complex [Mn(Cl)$(CO)_3$(H-DAB)], the oxidation of [Mn(Br)$(CO)_3$(iPr-DAB)] is largely localized on the p_π(Br)−d_π(Mn) HOMO (highest occupied molecular orbital) with a dominant contribution from the Br ligand. In contrast, the oxidation of the complex [Mn(Me)$(CO)_3$(iPr-DAB)] is localized on the HOMO possessing a d_π(Mn) character.[7] The σ(Mn−Me) bonding orbital then lies *ca.* 1 eV below the HOMO. On the other hand, the HOMO of [Mn(Bz)$(CO)_3$(iPr-DAB)] is a σ(Mn−Bz) orbital.[7] This apparent difference in the HOMO characters make the evaluation of the above $E_{p,a}$ trends rather difficult. The irreversible oxidation was not investigated in detail.

Discussion

(Spectro)electrochemistry of [Mn(X)(CO)$_3$(iPr-DAB)]^n (n = 0, X = Br, Me, Bz; n = +1, X = THF, MeCN, nPrCN, P(OMe)$_3$. The (spectro)electrochemical experiments described herein point to a facile dissociation of the non-carbonyl axial ligand from the primary one-electron reduction products [Mn(Br)$(CO)_3$(iPr-DAB)]$^{\bullet -}$ and [Mn(X)$(CO)_3$(iPr-DAB)]$^\bullet$ (X = THF, MeCN, nPrCN). These radical species could not be observed, even at 190 K and at ultrafast voltammetric scans. We have, however, shown that the transient 18e radicals [Mn(X)$(CO)_3$(iPr-DAB)]$^\bullet$ (X = donor solvent) are definitely involved in the reoxidation path of the ultimate two-electron reduction product [Mn$(CO)_3$(iPr-DAB)]$^-$ (see Scheme 1). Any reverse uptake of X by the transient radicals [Mn$(CO)_3$(iPr-DAB)]$^\bullet$ along the reduction path is prevented by their instantaneous one-

(38) Amatore, C. *J. Organomet. Chem. Libr.* **1990**, *22*, 1.

(39) The electrode potentials were determined against the cobaltocene/cobaltocenium couple, $CoCp_2^{0/+}$. The reported values are referred to the Fc/Fc$^+$ couple by using $E_{1/2}$ ($CoCp_2^{0/+}$) = −1.33 V *vs* Fc/Fc$^+$.

electron reduction producing the five-coordinate anions $[Mn(CO)_3(iPr\text{-}DAB)]^-$ directly at the reduction potental of the parent complexes. In contrast, the strong π-acceptor $P(OMe)_3$ ligand in $[Mn\{P(OMe)_3\}(CO)_3(iPr\text{-}DAB)]^\bullet$ remains bound rather firmly at low temperatures, and therefore, these radicals are detectable in the electrolyzed solution.

In contrast to $[Mn(X)(CO)_3(iPr\text{-}DAB)]^{\bullet -/-}$, the corresponding Re complexes[17] are significantly more stable. A similar conclusion can be drawn for other Mn and Re derivatives containing basic α-diimine ligands.[3a,b,13,40] Independent of the metal, the unpaired electron in these six-coordinate radicals is mainly localized on the lowest π^*(α-diimine) orbital.[3a,e,5,17,41] The very close ν(CO) wavenumbers of the radicals $[M(X)(CO)_3(\alpha\text{-diimine})]^\bullet$ (M = Mn, Re; X = PR_3, $P(OR)_3$)[3a,b,4,7] reflect comparable M → CO π-back-donation and, hence, a similar distribution of the electron density within the $(CO)_3M(\alpha\text{-diimine})$ fragment. The more efficient dissociation of the axial ligand X from $[Mn(X)(CO)_3(iPr\text{-}DAB)]^{\bullet -/-}$ relative to $[Re(X)(CO)_3(iPr\text{-}DAB)]^{\bullet -/-}$ may arise from a larger electron delocalization between the singly occupied π^*(α-diimine) and the σ^*(Mn-X) (*i.e.*, combined $p_z(X)$ and p_z, $d_{z^2}(Mn)$) orbitals, resulting in a stronger repulsion between the Mn center and the ligand X. The positive $\pi^*-\sigma^*$ overlap is assumed to increase substantially during an asymmetric distortion of $[Mn(X)(CO)_3(iPr\text{-}DAB)]^{\bullet -/-}$ caused[42] by an asymmetric stretching vibration of the radical complexes along the axial Mn−X bond. The stronger $\pi^*-\sigma^*$ interaction in the case of the radical Mn complexes may have its origin in the lower-lying and less diffuse σ^*(Mn−X) orbital compared to that of σ^*(Re−X).

The ECE(C) reduction path of $[Mn(X)(CO)_3(iPr\text{-}DAB)]^n$ (n = 0, X = Br; n = +1, X = THF, MeCN, nPrCN), analysed in detail in the Results (Scheme 1), is not unusual in organometallic electrochemistry. Suitable examples are the reduction of $[Fe(X)(CO)_3(\eta^3\text{-}C_3H_5)]$ (X = Cl, Br, I)[43] and $Fe(CO)_5$ or $Cr(CO)_6$ studied in detail by Amatore *et al.*[44] The common event along their reduction paths is generation of electron-deficient radicals whose dimerization cannot compete with their instantaneous reduction. Notably, a difference exists between the oxidation paths of the two-electron reduction products $[Fe(CO)_4]^{2-}$/$[Cr(CO)_5]^{2-}$ and $[Mn(CO)_3(iPr\text{-}DAB)]^-$. The one-electron-oxidized coordinatively unsaturated 17-electron radicals $[Fe(CO)_4]^-$ and $[Cr(CO)_5]^-$ directly dimerize. In contrast, the five-coordinate radicals $[Mn(CO)_3(iPr\text{-}DAB)]^\bullet$ have the odd electron localized on the iPr-DAB ligand[10,40] and should, therefore, be defined as formally 16-electron species $Mn^+(CO)_3(iPr\text{-}DAB^{\bullet -})$. Their direct dimerization is, therefore, a rather complex process[10] which apparently cannot compete efficiently with the alternative ECEC route to $[Mn(CO)_3(iPr\text{-}DAB)]_2$ depicted in Scheme 1.

No significant difference was observed between the reduction paths of $[Mn(X)(CO)_3(iPr\text{-}DAB)]$ (X = Me, Bz). Their lower reduction potentials relative to those of the other title complexes under study (see Table 2) reveal that the largely π^*(iPr-DAB) LUMO (lowest unoccupied molecular orbital) of these complexes[45] becomes considerably destabilized by coordination of the alkyl ligands. Regardless this trend, the one-electron-reduced products $[Mn(X)(CO)_3(iPr\text{-}DAB)]^{\bullet -}$ (X = Me, Bz) are apparently more stable than, *e.g.*, $[Mn(Br)(CO)_3(iPr\text{-}DAB)]^{\bullet -}$, as the radical anion with X = Me could even be detected by slow cyclic voltammetry. This difference is probably caused by a much higher energy of the σ^*(Mn−Me) orbital relative that of σ^*(Mn−Br), resulting in a weaker repulsive π^*(iPr-DAB)−σ^*(Mn−Me) interaction. The existence of the radical anionic intermediate along the reduction path leading directly to $[Mn(CO)_3(iPr\text{-}DAB)]^-$ (see eq 9) excludes the dissociation of the Me$^\bullet$ radical *via* the intramolecular dissociative electron-transfer reaction introduced by Savéant[46] on the model reaction R−X + e^- → R$^\bullet$ + X^- (R−X = alkyl halide).

Bonding Properties of $[Mn(CO)_3(iPr\text{-}DAB)]^-$ and Comparison with $[Mn(CO)_3(DBCat)]^-$. The ultimate closed-shell two-electron reduction product $[Mn(CO)_3(iPr\text{-}DAB)]^-$ is closely related to the five-coordinate anion $[Mn(CO)_3(DBCat)]^-$ [47] (DBCat is defined in ref 14). DFT-MO calculations performed[48] on the model compounds $[Mn(CO)_3(H\text{-}DAB)]^-$ and $[Mn(CO)_3(H\text{-}Cat)]^-$ confirm that substitution of the catecholate ligand by formally $[iPr\text{-}DAB]^{2-}$ with a considerably higher π^* level results in strongly changed HOMO and LUMO characters. The lowest electronic transition of $[Mn(CO)_3(H\text{-}Cat)]^-$ possesses a significant HCat → Mn LMCT character whereas that of $[Mn(CO)_3(H\text{-}DAB)]^-$ is largely delocalized, π(Mn−DAB) → π^*(Mn−DAB), with a rather limited charge-transfer character. This transition in $[Mn(CO)_3(iPr\text{-}DAB)]^-$ occurs at 490 nm, in agreement with 505 nm calculated[48] for $[Mn(CO)_3(H\text{-}DAB)]^-$. The DFT data also document that the negative charge on $[Mn(CO)_3(iPr\text{-}DAB)]^-$ is almost equally divided over the CO and iPr-DAB ligands, in contrast to $[Mn(CO)_3(DBCat)]^-$ where it mainly resides on the DBCat ligand.[47−49] This difference explains the considerably lower ν(CO) wavenumbers of $[Mn(CO)_3(iPr\text{-}DAB)]^-$ (see Table 2) in comparison with 1994 and 1891(br) cm^{-1} for the latter anion (in THF).[47] The effective oxidation-state distribution in the five-coordinate anion is best described as $[\{Mn(CO)_3\}^0(iPr\text{-}DAB^{-I})]^-$, with the Mn center bearing a partial positive charge. In contrast, the anion $[Mn(CO)_3(DBCat)]^-$ is a less π-delocalized, formally $Mn^I(DBCat^{-II})$ complex, which corresponds with its DBCat-localized one-electron oxidation, large ν(CO) wavenumbers, and tendency to reversibly form six-coordinate adducts with various Lewis bases.[47a,50]

Relation between Electrochemical and Photochemical Generation of $[Mn(CO)_3(\alpha\text{-diimine})]^-$. The photochemical formation of the five-coordinate

(40) Andréa, R. R.; de Lange, W. G. J.; van der Graaf, T.; Rijkhoff, M.; Stufkens, D. J.; Oskam, A. *Organometallics* **1988**, *7*, 1100.
(41) Stor, G. J.; Stufkens, D. J.; Vernooijs, P.; Baerends, E. J.; Fraanje, J.; Goubitz, K. *Inorg. Chem.* **1995**, *34*, 1588.
(42) (a) Vlček, A., Jr.; Víchová, J.; Hartl, F. *Coord. Chem. Rev.* **1994**, *132*, 167. (b) Bauman, F.; Grevels, F.-W.; Kaim, W.; Hartl, F.; Vlček A., Jr. *Inorg. Chim. Acta*, submitted for publication.
(43) Osella, D.; Ravera, M.; Kukharenko, S. V.; Strelets, V. V.; Housecroft, C. E. *J. Organomet. Chem.* **1991**, *417*, 421.
(44) Amatore, C.; Krusic, P. J.; Pedersen, S. U.; Verpeaux, J.-N. *Organometallics* **1995**, *14*, 640.
(45) Wilms, M. P. unpublished results. According to DFT MO calculations on the model complex $[Mn(Et)(CO)_3(H\text{-}DAB)]$, the reduction of $[Mn(X)(CO)_3(iPr\text{-}DAB)]$ (X = Me, Bz) is localized on a LUMO possessing a predominant π^*(iPr-DAB) character with a small contribution from the alkyl ligand.
(46) (a) Savéant, J.-M. *J. Am. Chem. Soc.* **1987**, *109*, 6788. (b) Savéant, J.-M. *Acc. Chem. Res.* **1993**, *26*, 455.
(47) (a) Hartl, F.; Stufkens, D. J.; Vlček A., Jr. *Inorg. Chem.* **1992**, *31*, 1687. (b) Hartl, F. *Inorg. Chim. Acta* **1995**, *232*, 99.
(48) Hartl, F.; Baerends, E. J.; Rossenaar, B. D.; Stufkens, D. J.; Wilms, M. P. *Inorg. Chem.*, manuscript in preparation.
(49) Hartl, F.; Vlček, A., Jr. *Inorg. Chem.* **1991**, *30*, 3048.
(50) Hartl, F. *Inorg. Chim. Acta*, in press.

Scheme 3

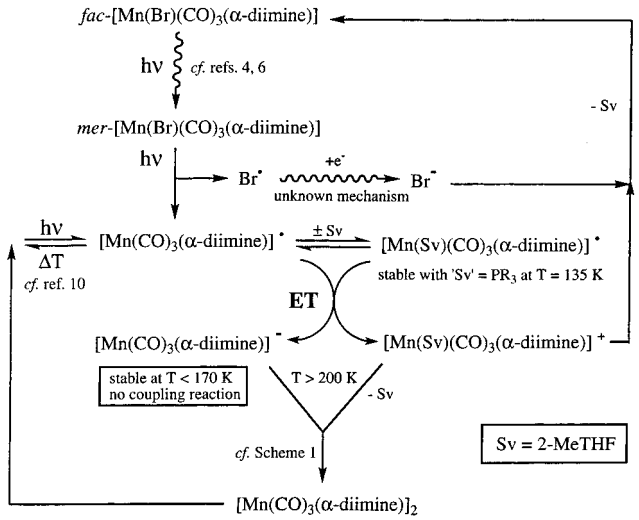

anions [Mn(CO)$_3$(α-diimine)]$^-$ (α-diimine = bpy, iPr-PyCa[15]) from *fac*-[Mn(X)(CO)$_3$(α-diimine)] (X = Br) proceeds *via* several intermediates, including *mer*-[Mn(Br)(CO)$_3$(α-diimine)] which further photodecomposes to reactive radicals [Mn(CO)$_3$(α-diimine)]$^\bullet$ and Br$^\bullet$.[4−6] Notably, irradiation of *mer*-[Mn(Br)(CO)$_3$(iPr-DAB)] only produces non-carbonyl species.[6]

The radicals [Mn(CO)$_3$(α-diimine)]$^\bullet$ are the key transients which link together the *photochemical* and *electrochemical* routes to [Mn(CO)$_3$(α-diimine)]$^-$ (see Scheme 3). A fraction of photogenerated [Mn(CO)$_3$(α-diimine)]$^\bullet$ can take up a solvent molecule. This process occurs even at room temperature, in agreement with the reoxidation path in Scheme 1. At $T = 135$ K this uptake remains the only possibility[10] as no dimer [Mn(CO)$_3$(α-diimine)]$_2$ was photochemically produced under such conditions.[4] In toluene, the radicals [Mn(CO)$_3$(R-DAB)]$^\bullet$ could be detected by EPR spectroscopy at $T = 200-250$ K[10,40]. This experimental evidence allows us to safely conclude that the [Mn(CO)$_3$(α-diimine)]$^-$ photoproduct originates from an electron transfer from the six-coordinate [Mn(X)(CO)$_3$(α-diimine)]$^\bullet$ (X = donor solvent) to the five-coordinate [Mn(CO)$_3$(α-diimine)]$^\bullet$ radicals present simultaneously in the solution (see Scheme 3). This disproportionation step is the characteristic event in the electrochemical DISP 1 sequence operating in the bulk solution (see eq 7). Importantly, in the presence of excess PR$_3$, the inherently stable 18e radicals [Mn(PR)$_3$(CO)$_3$(α-diimine)]$^\bullet$ are the only photoproducts at low temperatures.[4] Furthermore, the yield of [Mn(CO)$_3$(α-diimine)]$^-$ is negligible in very weakly coordinating toluene.[4] The photochemical disproportionation route to [Mn(CO)$_3$(α-diimine)]$^-$ apparently cannot operate under these circumstances.

The second disproportionation product [Mn(X)(CO)$_3$(α-diimine)]$^+$ (X = 2-MeTHF) probably converts back to parent *fac*-[Mn(Br)(CO)$_3$(α-diimine)] *via* a substitution reaction with Br$^-$, in analogy with the oxidation path in Scheme 1. It still remains unclear, however, how the primarily produced Br$^\bullet$ radicals transform to the corresponding anions. Recall that neither Br$^\bullet$ nor Br$_2$ were actually detected on irradiation of *mer*-[Mn(Br)(CO)$_3$(α-diimine)].[4]

At $T \geq 170$ K, photochemically produced [Mn(CO)$_3$(α-diimine)]$^-$ thermally convert into the dimer [Mn(CO)$_3$(α-diimine)]$_2$.[4] This is probably caused by the coupling reaction of the anions with unreacted parent *fac*-[Mn(Br)(CO)$_3$(α-diimine)], introduced here in Scheme 1. For α-diimine = iPr-DAB, we have shown that this reaction becomes largely inhibited already at $T \leq 200$ K, whereas lower temperatures are required for α-diimine = bpy.[13]

Conclusions

The detailed knowledge of the redox paths of the title complexes *fac*-[Mn(X)(CO)$_3$(iPr-DAB)]^n ($n = 0, +1$) and of the two-electron reduction product [Mn(CO)$_3$(iPr-DAB)]$^-$ provides an indispensable aid for the correct description of the electron-transfer events in the overall mechanism of the photochemical transformation of *fac*- and *mer*-[Mn(Br)(CO)$_3$(α-diimine)] into [Mn(CO)$_3$(iPr-DAB)]$^-$ and/or [Mn(CO)$_3$(iPr-DAB)]$_2$.

The key electro- and photochemical transients are the five-coordinate radicals [Mn(CO)$_3$(α-diimine)]$^\bullet$ whose redox behavior and reactivity toward Lewis bases markedly differ from those of the corresponding Re derivatives.

The ultimate photo and reduction product [Mn(CO)$_3$(iPr-DAB)]$^-$ can be considered as a strongly π-delocalized five-coordinate complex with the negative charge divided over the CO and iPr-DAB ligands.

Acknowledgment. The Dutch group thanks the Netherlands Foundation for Chemical Research (SON) and the Netherlands Organization for Scientific Research (NWO) for financial support. F.H. is also grateful to the J. H. van't Hoff Research Institute for financial support which covered his scientific stay at Ecole Normale Supérieure in Paris. The French group acknowledges partial support from CNRS, Ecole Normale Supérieure, and the French Ministry of Research.

Supporting Information Available: Figures 4, 6, 7B, and 9, showing IR spectra recorded during the reduction of [Mn(nPrCN)(CO)$_3$(iPr-DAB)]$^+$ at 198 K, cyclic voltammograms of [Mn(Br)((CO)$_3$(iPr-DAB)] (in THF) and [Mn(MeCN)(CO)$_3$(iPr-DAB)]$^+$ (at $v = 2$ V/s), and $E_{p,c}$ *vs* log(v) and $I_p v^{-1/2}$ *vs* log(v) functions of [Mn(X)(CO)$_3$(iPr-DAB)]^n ($n = 0$, X = Br; $n = +1$, X = THF), respectively (4 pages). Ordering information is given on any current masthead page.

OM9702791